Geophysical Research Letters

RESEARCH LETTER
10.1029/2020GL092262

1001 Rocket Launches for Space Missions and Their Infrasonic Signature

Christoph Pilger[1], **Patrick Hupe**[1], **Peter Gaebler**[1], **and Lars Ceranna**[1]

[1]Federal Institute for Geosciences and Natural Resources (BGR), Hanover, Germany

Key Points:

- We analyze 1001 rocket launches since 2009 using International Monitoring System infrasound arrays
- We estimate the global detectability, individual signal characteristics, and an amplitude-energy relation of rocket infrasound
- We provide a ground-truth data set of signal parameters for 7637 infrasound events from 733 launches

Supporting Information:

Supporting Information may be found in the online version of this article.

Correspondence to:

C. Pilger,
christoph.pilger@bgr.de

Citation:

Pilger, C., Hupe, P., Gaebler, P., & Ceranna, L. (2021). 1001 rocket launches for space missions and their infrasonic signature. *Geophysical Research Letters*, *48*, e2020GL092262. https://doi.org/10.1029/2020GL092262

Received 22 DEC 2020
Accepted 17 MAR 2021

Author Contributions:

Conceptualization: Christoph Pilger
Data curation: Christoph Pilger, Patrick Hupe
Formal analysis: Patrick Hupe
Investigation: Christoph Pilger
Methodology: Patrick Hupe
Project Administration: Lars Ceranna
Resources: Peter Gaebler
Software: Peter Gaebler
Supervision: Lars Ceranna
Validation: Christoph Pilger, Lars Ceranna
Visualization: Patrick Hupe, Peter Gaebler

Abstract Infrasound array processing is applied to monitor and characterize atmospheric explosions in the context of the Comprehensive Nuclear-Test-Ban Treaty. Anyhow, for many infrasound sources the exact location and time are initially unknown and sometimes difficult to precisely estimate afterward. In contrast, rocket launches are well-defined ground-truth events generating strong infrasonic signatures. During the last decade, the number of rocket launches for sending satellites into Earth's orbit and for reaching space strongly increased. We collected ground-truth information for 1001 rocket launches from 27 global spaceports between 2009 and mid-2020 and were able to identify infrasound signatures from up to 73% of the launches on the International Monitoring System of infrasound stations. We use these unique data to estimate the global detectability of such events, to characterize rocket infrasound, to derive an amplitude-energy relation, and to provide the results for further use as a ground-truth reference in geophysical and atmospheric research.

Plain Language Summary The launching of rockets from spaceports like Cape Canaveral, USA or Baikonur, Kazakhstan produces extremely loud sounds that can be heard at large distances. Similar to the basses of a large concert there are deep sounds that travel even farther, up to thousands of kilometers, through the air. This sound below what humans can hear, so called infrasound, can be collected by extremely sensitive instruments, similar to microphones for recording music. Within our study we were able to identify the sound of 733 out of 1001 rocket launches, performed within more than a decade of spaceflights, to bring satellites, astronauts, or cargo into space. We look at the tone of these starts to find out which types of rockets are best detected at which infrasound stations; and why. We furthermore make our findings available for scientists that want to learn more about the rockets that produce the sound, the air that transports it, and the instruments that record it.

1. Introduction

Orbital spaceflights have been performed since the first Sputnik satellite launched in 1957, and Yuri Gagarin became the first human to reach space in 1961. Mankind performed the first Moon landing in 1969 and started crewing space stations in 1971. Currently, the only space station in Earth's orbit is the International Space Station (ISS). It started operation in 1998 and has permanently been crewed since 2000. It is regularly targeted by space missions for supply transports and crew exchanges. Numerous rocket launches are necessary to support the upkeep of the ISS, to bring orbital satellites and exploration probes into space, and to enable missions to Moon, Mars, and beyond.

Rocket launches for space missions are currently realized using vessels with propulsion engines and boosters having thrusts of hundreds to thousands of kilonewton (kN). They accelerate the rockets and their tons of payload by reactive mass expulsion of burned fuel to velocities sufficient for overcoming Earth's gravitational influence. The ignition, burning, and re-entry of rocket stages as well as the Mach cone from super-sonic velocities generate large-amplitude pressure perturbations and shock waves (Cotten & Donn, 1971; Donn et al., 1968; Kaschak et al., 1970). Similar to atmospheric explosions (Ceranna et al., 2009; Koch & Pilger, 2020; Vergoz et al., 2019) and meteoroids entering Earth's atmosphere (Le Pichon et al., 2013; Pilger et al., 2019; Silber et al., 2018), these source processes generate infrasonic signals detectable at stations at distances of hundreds to thousands of kilometers (Le Pichon et al., 2010; Pilger et al., 2017). Apart from the primary use to advance telecommunication and the human knowledge of Earth and space, these rocket launches for space missions also provide a large and unique data set of controlled, ground-based infrasound sources.

Writing – original draft: Christoph Pilger, Patrick Hupe
Writing – review & editing: Peter Gaebler

Previous studies on infrasound from rocket launches were performed during the early years of space missions (Balachandran & Donn, 1971; Balachandran et al., 1971; Cotten & Donn, 1971; Donn et al., 1968, 1971, 1975; Kaschak, 1969; Kaschak et al., 1970; McCarty & Dalins, 1971; Tahira & Donn, 1983). Many of them cover infrasound observations of the Saturn V rocket starts for the Apollo program, up to now the largest and heaviest space launches ever performed. Rocket infrasound studies in later years became sparse until the opening for signature of the Comprehensive Nuclear-Test-Ban Treaty (CTBT) in 1996 and the selection of infrasound as monitoring technique of its International Monitoring System (IMS) (Dahlman et al., 2009; Der et al., 2002). More recent infrasound studies include the detection and characterization of signatures from rocket types (e.g., Space Shuttle, Delta, Atlas, and Falcon rockets) that were still in operation during the observation period of this study (McLaughlin et al., 2000; McNutt et al., 2017; Olson, 2012; Smith et al., 2018; Tenney et al., 2003).

For the present study, we investigate infrasound signatures of a total of 1001 rocket launches for space missions between early 2009 and mid-2020 recorded at globally distributed IMS infrasound arrays. We include all surface- or ocean platform-based launches from the 27 active spaceports within these 11.5 years with known start time, location, rocket type, and mission name. Infrasound from the launches of sounding rockets (Blom et al., 2016) as well as ballistic missiles (Evers et al., 2018) for suborbital scientific and military purposes are not part of this study.

The central goals of our study are (i) the evaluation of the general and individual detectability of rocket infrasound at IMS stations, (ii) the estimation of rocket signal characteristics like the separation of different phases of the rocket launches using different processing and quality criteria, and (iii) the derivation of a relation between rocket thrust energy and observed acoustic amplitude as a first scientific application of the data set. By providing the ground-truth information of all rocket launches used in this study as well as the related infrasound findings as a DOI data set (Hupe et al., 2021), we furthermore aim at supporting future studies for source localization, signal characterization, calibration and validation purposes, as well as atmospheric dynamics research.

2. Data and Processing

The initial database of this study are 1001 rocket launches for space missions between January 1, 2009 and June 30, 2020. A comprehensive list of these starts with event date and UTC time, spaceport location, rocket type, and mission name is provided as supporting information to this study (Hupe et al., 2021). The rocket starts were conducted at 27 different spaceports (25 land-based facilities and two open-sea platforms), listed in Table S1 in Section S1. Seventy-six different types of rockets of individual size and engine thrust configuration contribute to the data set, as specified in Table S2 in Section S1. We consider differential pressure data from all certified and operational IMS infrasound arrays (42 stations in early 2009, increasing to 52 stations in mid-2020) with regard to rocket infrasound signatures during each of the 1001 space launches. Figure 1a shows the location of all certified IMS stations and spaceports with launch activity between 2009 and mid-2020.

For automatically detecting infrasound events related to the 1001 rocket launches, we examine the bulletins of IMS infrasound stations that were obtained from the comprehensive reprocessing of their waveform data using the Progressive Multi-Channel Correlation (PMCC) algorithm (Cansi, 1995; Cansi & Le Pichon, 2008; Le Pichon & Cansi, 2003). PMCC enables the detection of coherent plane waves within the background noise in successive, overlapping time windows and adjacent frequency bands. Here, the broadband processing configuration consisted of 27 third-octave frequency bands (Garcés, 2013) between 0.01 and 4 Hz and window lengths between 600 s and around 30 s, respectively. This enables accurate estimates of frequency-dependent wave parameters – for example, back azimuth and apparent velocity – that are derived from the time delays between pairs of sensor triplets of the array (Ceranna et al., 2019). Adjacent signal arrivals in individual time-frequency cells that exhibit similar parameters are clustered into a family of detections (Brachet et al., 2010). These families are assumed to be infrasound events, which are collected in the archived event lists of each station.

Here, we focus on center frequencies between 0.7 and 2.0 Hz. This frequency range covers the previously reported range of dominant energy (0.1–2 Hz; e.g., Kaschak et al., 1970) but avoids misattribution of globally

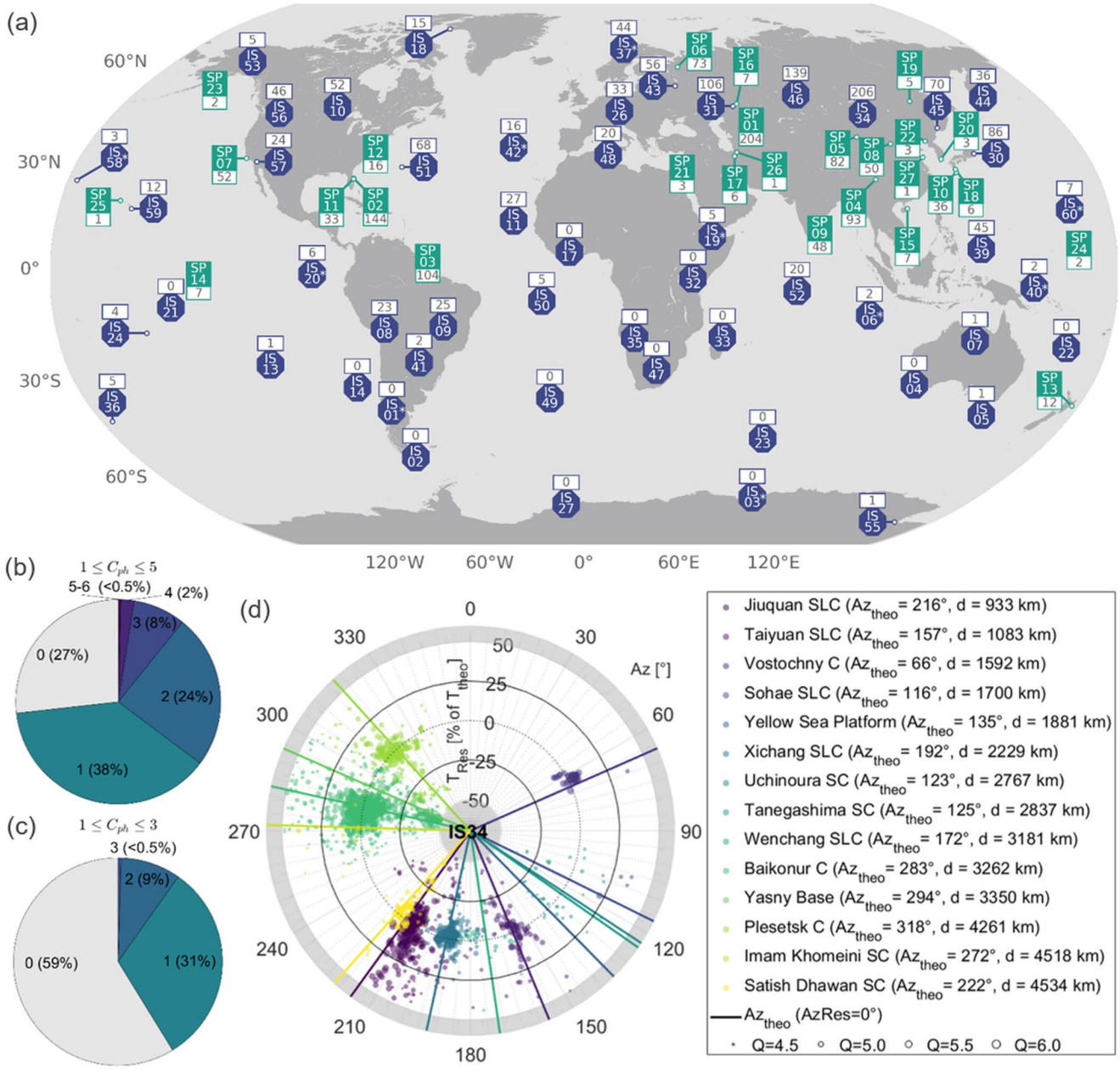

Figure 1. (a) Location of infrasound stations and spaceports; blue octagons mark the location of certified IMS infrasound arrays (station number within the marker, asterisk indicating certification after 2009), numbers above quantify the detected rocket launches; green squares show the locations of the 27 spaceports considered in this study (spaceport number following Table S1 within the marker), numbers below quantify the launches from that particular spaceport. (b), (c) Statistics of the data set: The pie charts show the portion of launches (in %) that are potentially detected by the indicated number of infrasound stations; for (b) all launch phases ($C_{ph} \leq 5$) and (c) more likely the liftoff or adjacent phases ($C_{ph} \leq 3$). (d) The distribution of all detections at IS34 ($C_{ph} \leq 5$) shows 2253 signatures of up to 206 rocket launches within the accepted range of azimuth and time residuals; solid lines indicate the theoretical directions to the associated spaceports, which are sorted and colored by increasing distance (for full spaceport names and numbers see Table S1); the signatures are denoted by 50% transparent dots such that intense colors highlight accumulations of signatures. IMS, International Monitoring System.

and quasi-continuously detected microbaroms (dominant range 0.1–0.6 Hz; e.g., Assink et al., 2014; Ceranna et al., 2019; Landès et al., 2014). In addition to the frequency, we apply two sets of criteria that an event must meet to qualify for one of the 1001 rocket launches. First, events that strongly deviate from theoretical detection times (>2 h) and back azimuths (>40°) are discarded while for each launch only IMS stations in the vicinity of 5,000 km of the spaceport are considered.

For the remaining events, we incorporate one-dimensional (1D) atmospheric profiles to correct the back azimuths for cross-wind effects and estimate celerities (details are given in Section S2). The second criteria set is based on three additional parameters that we introduce to assess the quality of a signature:

Q – a quality indicator ranging from 0 (low) to 6 (high), which is a sum of weighting functions for detection parameters (travel time residual T_{Res}, azimuth residual Az_{Res}, number of arrivals per event) and propagation quantities (effective sound speed ratios, distance), each ranging from 0 to 1 as defined and explained in Section S2.1, N_{Az} – an indicator for the uniqueness of a detection in terms of other sources and coherent background noise (Section S2.2), C_{ph} – an index ranging from 1 to 6 classifying the potential phase of the launch (Section S2.3).

The latter indicates whether a detection can be very likely attributed to the liftoff phase (1) or to another source including coherent noise (6). The azimuth indicator N_{Az}, which is based on the comprehensive bulletin lists and stacked monthly histograms from 2009 to 2020, provides an important ratio in this context.

In the final database provided with this manuscript (Hupe et al., 2021), we have sorted out all detections assigned with $C_{\mathrm{ph}} = 6$, which very likely represent directions of regularly occurring detections (on average, four times a day; see Section S2.3). Overall, our aim is to provide a sensitive data set with a low false association rate while disregarding as few true detections as possible. The introduced quality parameter Q therefore particularly focuses on those values that can be associated to the initial start phase and high signal content. Also, the criteria are further sharpened in this regard using the azimuth and travel time residuals ($\left|Az_{\mathrm{Res}}\right| < 30°$, $\left|T_{\mathrm{Res}} \,/\, T_{\mathrm{theo}}\right| \leq 50\%$) and $Q > 4.5$ (details given in Section S2).

The final data set of signatures that are deemed to be related to rocket launches contains 7637 entries. All parameters provided in the database are listed in Section S3. The number of potentially detected launches per IMS infrasound station is depicted in Figure 1a. The data set can be further constrained to the user's requirements. Among others, the classification index will be useful to do so.

3. Results

3.1. Event Detectability and Station Performance

The data set consists of 7637 infrasonic signatures from 733 different launches detected at 37 IMS infrasound stations; hence, it covers around 73% of the 1001 rocket launches while only 27% are not assigned to an infrasound detection within 5,000 km (Figure 1b). Around one third of the launches are potentially detected by two or more stations. When rather focusing on the initial start phase ($C_{\mathrm{ph}} \leq 3$, Figure 1c), for 59% of the launches no signature remains and only around 10% are detected at more than one IMS station. Nevertheless, the false association rate among these 2542 signatures that are allocated to 25 IMS stations is deemed to be significantly reduced. The 1394 signatures classified as being most likely related to the initial start phase ($C_{\mathrm{ph}} = 1$) spread over 10 IMS stations and only cover 24% of the rocket launches. Only one of these (launch event no. 680 in the data set) reveals signatures at two different stations (IS31 and IS34). This launch of a Soyuz rocket at Baikonur on April 19, 2013 is also listed in the Reviewed Event Bulletin (REB) of the CTBT Organization's International Data Centre, like many of the covered events are. For this event, the near-real-time REB analysis additionally contains IS53, which is beyond the 5,000 km threshold, and IS46, for which our data set reveals signatures with $C_{\mathrm{ph}} = 4$ (potential post-liftoff phase). The partition of the infrasound signatures to the classification indices is given in Section 2.3.

The majority of spaceports and also rocket launches are located in central and eastern Asia, therefore, stations with the most rocket infrasound detections are also located there (IS34, Mongolia; IS45 and IS46, Russia; IS31, Kazakhstan; IS30, Japan, see Figure 1a). These are followed by detections of spacecraft launches at Cape Canaveral and Kennedy Space Center (Florida, USA), predominantly observed at IS51, Bermuda, and other sites in North America. We highlight two specific rocket launch events recorded at infrasound array IS51 in Section 3.2. Infrasound arrays certified later than the starting date of this study (indicated by asterisks in Figure 1a) tend to have fewer detections compared to neighboring stations since they are in operation only a fraction of the investigated period. Detections from infrasound arrays in the Southern Hemisphere are generally sparse because there are nearly no spaceports and rocket launch activities.

We present an overview of rocket launch recordings at infrasound array IS34, having the most rocket infrasound detections globally (2253 signatures of 206 launches from 14 different spaceports), in Figure 1d ($C_{ph} \leq 5$). The signature distribution within the accepted time and azimuth residuals at IS34 highlights accumulations around $T_{Res} = 0$ s and $Az_{Res} = 0°$ for 7 of the 14 associated spaceports in different directions of the station, indicating that these signatures are likely related to the initial launch phases. The majority of all signatures are detected between October and April (93.4%), when the Northern Hemisphere stratospheric circulation favors eastward propagation. Indeed, nearly all signatures originating from Baikonur (SP01) and Plesetsk Cosmodromes (SP06) fell into this period, accordingly with effective sound speed ratios (i.e., the wind-dependent sound speed at around 50 km relative to the sound speed at the ground) around or exceeding one, which is conducive for detections.

The summertime signatures detected at IS34 only amount to 1.3% dating from June to August. One half of these originate from spaceports located to easterly (Vostochny Cosmodrome, SP19) or south-easterly directions (Taiyuan Satellite Launch Center, SP08) with effective sound speed ratios around 1.1. The other half originates from southerly to south-westerly directions, including the Jiuquan Satellite Launch Center (SP05). The lower effective sound speed ratios (0.92–0.96) are compensated by small azimuth residuals ($Az_{Res} \leq 5°$) and large family sizes (200).

In addition to the seasonal dependency, we also identify a day time tendency for increased detection numbers. Around 60% of the signatures are detected during night time (18:00 till 06:00 local time). In contrast, only 19% of the signatures date from the afternoon (12:00–18:00 local time), when the noise level is generally increased due to local turbulence and human activities (e.g., from Ulaanbaatar, 35 km in the east-northeast). Station-specific ambient noise has a strong influence on the detection performance of IMS infrasound arrays (e.g., Matoza et al., 2013).

The only pattern of accumulations at larger time residuals is found for Baikonur Cosmodrome (SP01) at around −40%, which could reflect signatures of secondary booster ignitions after a spacecraft lifted off towards the east and thus approached IS34. Constraining the classification index to values of 1–3 sorts out the majority of scattered signatures at larger residuals as well as those from eight spaceports completely (see Figure S2). Also the aforementioned pattern disappears because the related database entries are assigned $C_{ph} = 4$, hence neither fulfilling the liftoff criteria nor representing repeating directions of likely other origin.

The rigorous criteria for classification indices of 1–3 are deliberately chosen (Section S2.3) to focus on potential liftoff signatures with different confidence levels (depending on the indicator N_{Az}). We focus on the upper 15% of propagation and detection conditions with $Q > 5.1$ while strictly limiting the relative time residual to 15% and the azimuth residual to 5° accordingly – although cross-wind effects are known that can alter the back azimuth by up to 10° (e.g., Le Pichon et al., 2005). Nevertheless, deviations due to propagation effects have already been incorporated using the 1D model correction and celerity estimation (see Section S2). Consequently, the residuals should rather be lower than the chosen tolerances; however, these account for additional uncertainties potentially introduced by the 1D profiles for long-range propagation up to 5,000 km, if the atmospheric conditions vary along the paths. Overall, this amount of significantly varying conditions between the spaceport and the receiving station is deemed small: Both effective sound speed ratios equal or exceed 1 for more than 79% of the database.

3.2. Rocket Infrasound Signatures

While the 1001 rocket launches of this study are automatically analyzed by the PMCC method and categorized by the given criteria, we present a detailed comparison of two rocket launches in Figure 2. The flights of a Space Shuttle on November 16, 2009 and of a Falcon 9 rocket on January 7, 2020 are recorded at the IMS infrasound array IS51 (Bermuda) at 1580 km distance. Both rockets performed their liftoff from Cape Canaveral/Kennedy Space Center, Florida, USA, with a space ascent into northeastern direction and their ejected boosters landing in the North Atlantic Ocean between the US coast and Bermuda Island.

We identified the infrasonic signatures of both rocket starts and the booster landings in the IS51 recordings. Since the rockets move towards Bermuda and quickly reach supersonic flight velocities, their later flight

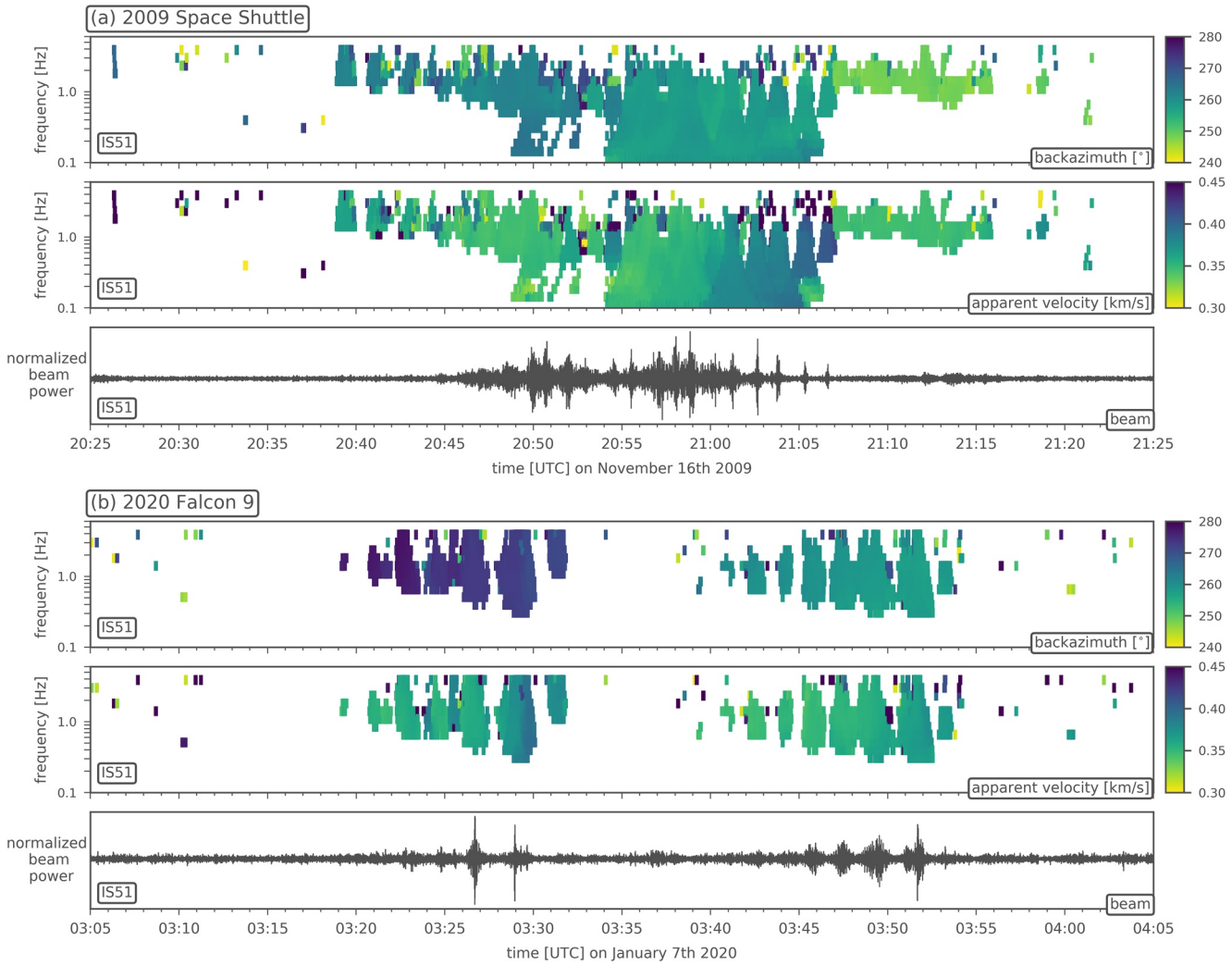

Figure 2. PMCC analysis of IMS infrasound array IS51 (Bermuda) for a 2009 Space Shuttle (a) and a 2020 Falcon 9 (b) rocket launch. Shown in the corresponding top frames are the observed back azimuths within ±20° of the true direction towards the launch facility (Cape Canaveral/Kennedy SC, $Az_{theo} = 259°$), in the middle frames the observed apparent velocities, and in the bottom frames the waveform beams, which are bandpass-filtered between 0.5 and 5 Hz. IMS, International Monitoring System; PMCC, Progressive Multi-Channel Correlation.

and booster landing signals arrive at Bermuda before the launch and initial flight signals. This is accompanied by a Doppler effect (Blom et al., 2016; Olson, 2012), where signals from a movement towards the observing station show a frequency increase (in Figure 2: Backward in time, since later signals come before earlier ones).

For the Space Shuttle, we observe impulsive signals from the solid fuel booster ignition (Blom et al., 2016; Olson, 2012) and ascent between 20:54 and 21:07 UTC, characterized by increasing apparent velocities from left to right, indicative of signal returns from increasing altitudes as time progresses (Pilger et al., 2020; Silber et al., 2018). These are preceded by a second group of signals following the booster separation and descent between 20:45 and 20:53 UTC and a third, weak signature probably from booster splashdown between 20:39 and 20:44 UTC. Signals after 21:07 UTC are originating from a different direction and are most likely from another source (e.g., local surf or anthropogenic noise).

For the Falcon 9 start, we find similar features, though the used liquid fuel produces less impulsive acoustic waveform signatures (Olson, 2012). The launch (03:40 to 03:54 UTC) and separation/landing (03:19 to 03:32 UTC) parts of the signal are divided by a larger time interval due to the fact that the landing area for the boosters is farther away from the launch site and nearer to Bermuda. The landing of the Falcon 9 boosters

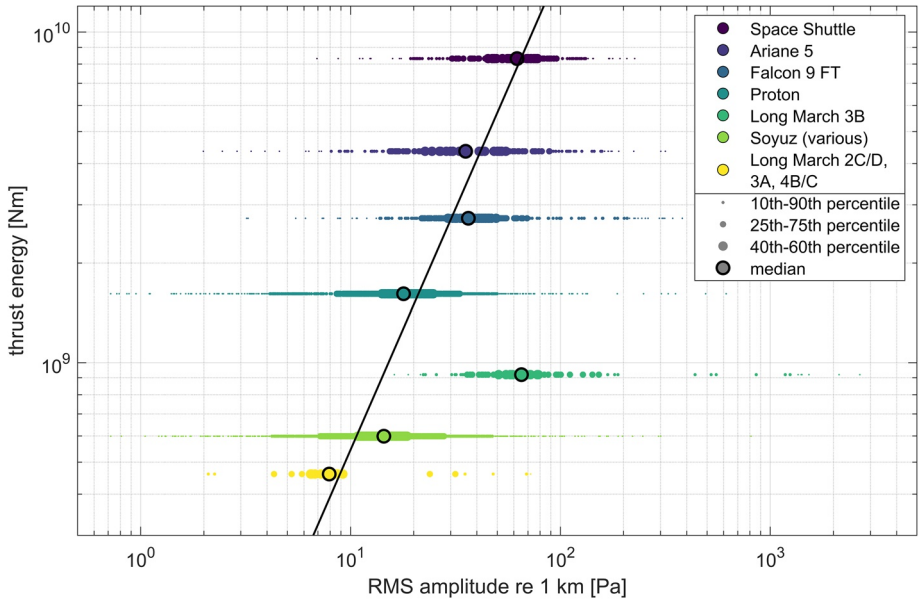

Figure 3. Estimation of rocket energy released during the first stage against measured RMS amplitudes corrected for distance and propagation conditions. The outlier Long March 3B is neglected for calculating the fit (solid line), which depicts the median-based relation given in Equation 1. RMS, root-mean-square.

was realized on a floating ocean platform, which explains stronger landing signals due to another booster ignition for slowing down and touchdown.

These two examples show that different phases of the rocket launch contribute to the infrasound signatures and that they can in principle be separated by the $C_{ph} \leq 3$ (azimuth within ±5°, time residual within ±15%, here about 13 min) and $C_{ph} = 4$ criteria. Furthermore, all signals are also subject to infrasonic multipathing, where repetitive signal groups and pulses are observed arriving at the array from different propagation paths and reflection altitudes (Ceranna et al., 2009; Vergoz et al., 2019). This explains that five to ten different waveform pulses and signal families are observed for each flight phase (starting and ascent, booster separation, descent and landing). These are not necessarily due to different source effects like single engine bursts, rocket stage separations and sonic booms, but due to the separation of signal energy along different propagation paths, mainly occurring after long-range propagation (here 1580 km) in a stratospheric waveguide. It is noteworthy that almost all pulses cover the frequency range between 0.7 and 2 Hz that was chosen for the automated analyses.

3.3. Amplitude-Energy Relation

For a first application of the data set, we demonstrate an energy estimation as a function of measured root-mean-square (RMS) amplitudes. We focus on the first stage of a launch and the most likely associated signatures ($C_{ph} = 1$). We select six different thrust levels of (grouped) rocket types that were launched at least 50 times, plus the Space Shuttle with the largest thrust (11 launches within the period). The released energy is estimated using the rocket equation (details in Section S4), incorporating thrust, boost time, and exhaust velocity of the burned mass (Table S2). Also, we assume a unified mass ratio of before boost ignition and after boost time to be 3.5.

For each of the 1146 signatures of the seven rocket types, the RMS amplitude is twice corrected (re 1 km) by a frequency- and distance-dependent attenuation coefficient (Le Pichon et al., 2012, their Equation 2) using the effective sound speed ratio determined at (i) the station and (ii) the spaceport. When plotting the resulting amplitudes ($A_{RMS,re\ 1\ km}$) against the estimated energy (Figure 3), the Long March 3B (LM3B) amplitudes do cohesively not fit into the overall pattern for unknown reasons. The median amplitude deviates by around four times from Soyuz and other LM types, thus being comparable to the Space Shuttle, which releases ninefold energy. All LM3B signatures are detected at IS34; this station is among the nine stations

the other rocket types are detected at, while no station-specific bias is recognized. We, therefore, disregard LM3B for proposing a robust, median-based relation between RMS amplitude and energy (E) released during the first launch phase:

$$\log_{10}(E) = 1.458 \cdot \log_{10}\left(A_{\mathrm{RMS,re\,1\,km}}\right) + 7.278 \quad (1)$$

This equation matches the 40th-to-60th-percentile ranges (Figure 3) of rockets that cover thrusts of between 2,962 and 30,250 kN (Table S2). These percentiles differ by a factor of two per rocket type, whereas the total amplitude range spans over more than one magnitude order. Such uncertainties are not uncommon for infrasound-based yield/energy relations for explosion-like sources (Golden et al., 2012) because of underlying assumptions concerning propagation and detection conditions and source characteristics. We point out three simplified assumptions leading to Equation 1. (i) Effective sound speed ratios are derived from 1D atmospheric profiles (spaceport and receiver). (ii) Acoustic signals are generated solely by the engine boost (e.g., see Koch, 2010; Pilger et al., 2013) and not also the possible supersonic boom. The thrust energy is considered in direct relation to the acoustic signals, without considering efficiency. (iii) Only the first stage rocket parameters are considered and no height adjustment is conducted (decreasing density); any possibly more effective high-altitude emission is not considered.

Overall, rocket launch characteristics are more complex than explosions and not a point source; hence, our focus on the initial start phase. Although this implies that – despite the introduced quality parameters – single signatures could be unrelated to a rocket launch, Equation 1 provides a first robust estimate, which serves as a foundation for more detailed investigations using this data set.

4. Conclusions

From a total of 1001 rocket launches during 11.5 years of observation, we collect a data set of 7637 infrasound signatures recorded at global IMS infrasound arrays. This data set enables us to derive detailed signal characteristics of rocket infrasound, on the one hand by proving signal parameters derived from our PMCC processing and on the other hand by applying criteria developed for distinguishing different launch phases and separating rocket infrasound from other potential noise sources.

Our derived data set, therefore, serves as a ground-truth reference for estimating the global detectability of rocket infrasound in general and for validating the individual station performance of IMS arrays to detect the given events. We highlight the importance of precise atmospheric background modeling, implementing high-resolution atmospheric model analysis data, for the localization and characterization of these ground-truth events also with respect to seasonal and diurnal variations. We finally derive a distance- and propagation-corrected relation between rocket thrust energy and acoustic amplitude that enables us to provide a first estimate of the expected acoustic signal solely depending on rocket specifications. A detailed investigation could make a significant contribution towards introducing an infrasound magnitude.

While we do not exhaustively analyze the given data set for any potential dependencies on signal parameters, atmospheric propagation, and station quality, we, nevertheless, provide it as a reference database for future studies about infrasound acoustics and atmospheric dynamics.

Conflict of Interest

The authors declare no conflicts of interest relevant to this study.

Data Availability Statement

The event list of 1001 rocket launches with their time, location, rocket type, and mission information as well as the detection list of 7637 infrasound signatures with their processing and quality parameters are available as supporting information to this study (https://doi.org/10.25928/bgrseis_1001-ifsd; Hupe et al., 2021). Access to the IMS network's data such as differential pressure recordings of the infrasound stations are available to National Data Centers of the CTBTO and can be made available to others on request at https://

www.ctbto.org/specials/vdec (last accessed on December 14, 2020). The operational high-resolution atmospheric model analysis, defined by the Integrated Forecast System of the European Centre for Medium Range Weather Forecast (ECMWF), is available at https://www.ecmwf.int/en/forecasts/datasets (last accessed on December 14, 2020). Rocket launch information was collected using the "Spaceflight Now" catalog and archive at https://spaceflightnow.com/(last accessed on December 14, 2020). Spaceport information was accessed using the "Spaceports of the World" report available at https://aerospace.csis.org/spaceports-of-the-world/(last accessed on December 14, 2020). Information about different rocket types and their payload and thrust were collected using the "Encyclopedia Astronautica" at http://www.astronautix.com, "Wikipedia" at https://en.wikipedia.org/wiki/Comparisonand "Gunters Space Page" at https://space.skyrocket.de/ (all last accessed December 14, 2020).

Acknowledgments
The authors are grateful for the constructive reviews by Alex Iezzi and an anonymous reviewer.

References

Assink, J. D., Waxler, R., Smets, P., & Evers, L. G. (2014). Bidirectional infrasonic ducts associated with sudden stratospheric warming events. *Journal of Geophysical Research: Atmosphere*, *119*, 1140–1153. https://doi.org/10.1002/2013JD021062

Balachandran, N. K., & Donn, W. L. (1971). Characteristics of infrasonic signals from rockets. *Geophysical Journal International*, *26*(1–4), 135–148. https://doi.org/10.1111/j.1365-246X.1971.tb03387.x

Balachandran, N. K., Donn, W. L., & Kaschak, G. (1971). On the propagation of infrasound from rockets: Effects of winds. *Journal of the Acoustical Society of America*, *50*(2A), 397–404. https://doi.org/10.1121/1.1912649

Blom, P., Marcillo, O., & Arrowsmith, S. (2016). Analysis and modeling of infrasound from a four-stage rocket launch. *Journal of the Acoustical Society of America*, *139*(6), 3134–3138. https://doi.org/10.1121/1.4953817

Brachet, N., Brown, D., Le Bras, R., Cansi, Y., Mialle, P., & Coyne, J. (2010). Monitoring the Earth's atmosphere with the Global IMS infrasound network. In *Infrasound monitoring for atmospheric studies* (pp. 77–118). Springer. https://doi.org/10.1007/978-1-4020-9508-5\text{_}3

Cansi, Y. (1995). An automatic seismic event processing for detection and location: The PMCC method. *Geophysical Research Letters*, *22*(9), 1021–1024. https://doi.org/10.1029/95GL00468

Cansi, Y., & Le Pichon, A. (2008). Infrasound event detection using the progressive multi-channel correlation algorithm. In *Handbook of signal processing in acoustics* (pp. 1425–1435). Springer. https://doi.org/10.1007/978-0-387-30441-0\text{_}77

Ceranna, L., Le Pichon, A., Green, D. N., & Mialle, P. (2009). The Buncefield explosion: A benchmark for infrasound analysis across Central Europe. *Geophysical Journal International*, *177*(2), 491–508. https://doi.org/10.1111/j.1365-246X.2008.03998.x

Ceranna, L., Matoza, R., Hupe, P., Le Pichon, A., & Landès, M. (2019). Systematic array processing of a decade of Global IMS infrasound data. In *Infrasound monitoring for atmospheric studies* (pp. 471–482). Springer. https://doi.org/10.1007/978-3-319-75140-5\text{_}13

Cotten, D., & Donn, W. L. (1971). Sound from Apollo rockets in space. *Science*, *171*(3971), 565–567. https://doi.org/10.1126/science.171.3971.565

Dahlman, O., Mykkeltveit, S., & Haak, H. (2009). *Nuclear test ban: Converting political visions to reality*. Springer Science & Business Media.

Der, Z. A., Shumway, R. H., & Herrin, E. T. (2002). Monitoring the comprehensive nuclear-test-ban treaty: Data processing and infrasound. In *Pageoph Special Issue*. Springer.

Donn, W. L., Balachandran, N. K., & Rind, D. (1975). Tidal wind control of long-range rocket infrasound. *Journal of Geophysical Research*, *80*(12), 1662–1664. https://doi.org/10.1029/JC080i012p01662

Donn, W. L., Dalins, I., McCarty, V., Ewing, M., & Kaschak, G. (1971). Air-coupled seismic waves at long range from Apollo launchings. *Geophysical Journal International*, *26*(1–4), 161–171. https://doi.org/10.1111/j.1365-246X.1971.tb03389.x

Donn, W. L., Posmentier, E., Fehr, U., & Balachandran, N. K. (1968). Infrasound at long range from Saturn V, 1967. *Science*, *162*(3858), 1116–1120. https://doi.org/10.1126/science.162.3858.1116

Evers, L. G., Assink, J. D., & Smets, P. S. (2018). Infrasound from the 2009 and 2017 DPRK rocket launches. *Geophysical Journal International*, *213*(3), 1785–1791. https://doi.org/10.1093/gji/ggy092

Garcés, M. A. (2013). On infrasound standards, Part 1: Time, frequency, and energy scaling. *InfraMatics*, *2*, 13–35. http://dx.doi.org/10.4236/inframatics.2013.22002

Golden, P., Negraru, P., & Howard, J. (2012). *Infrasound studies for yield estimation of HE explosions* (Technical Report). Southern Methodist University.

Hupe, P., Pilger, C., Gaebler, P., & Ceranna, L. (2021). *Infrasonic signatures of 1001 rocket launches for space missions* [data product]. Federal Institute for Geosciences and Natural Resources. https://doi.org/10.25928/bgrseis_1001-ifsd

Kaschak, G. (1969). Long-range supersonic propagation of infrasonic noise generated by missiles. *Journal of Geophysical Research*, *74*(3), 914–918. https://doi.org/10.1029/JA074i003p00914

Kaschak, G., Donn, W. L., & Fehr, U. (1970). Long-range infrasound from rockets. *Journal of the Acoustical Society of America*, *48*(1A), 12–20. https://doi.org/10.1121/1.1912102

Koch, K. (2010). Analysis of signals from a unique ground-truth infrasound source observed at IMS station IS26 in Southern Germany. *Pure and Applied Geophysics*, *167*, 401–412. https://doi.org/10.1007/s00024-009-0031-2

Koch, K., & Pilger, C. (2020). A comprehensive study of infrasound signals detected from the Ingolstadt, Germany, explosion of 1 September 2018. *Pure and Applied Geophysics*, *177*, 1–17. https://doi.org/10.1007/s00024-020-02442-y

Landès, M., Le Pichon, A., Shapiro, N. M., Hillers, G., & Campillo, M. (2014). Explaining global patterns of microbarom observations with wave action models. *Geophysical Journal International*, *199*(3), 1328–1337. https://doi.org/10.1093/gji/ggu324

Le Pichon, A., Blanc, E., Drob, D., Lambotte, S., Dessa, J., Lardy, M., & Vergniolle, S. (2005). Infrasound monitoring of volcanoes to probe high-altitude winds. *Journal of Geophysical Research*, *110*(D13106), D13106. https://doi.org/10.1029/2004JD005587

Le Pichon, A., Blanc, E., & Hauchecorne, A. (2010). *Infrasound monitoring for atmospheric studies*. Springer Science & Business Media. https://doi.org/10.1007/978-1-4020-9508-5

Le Pichon, A., & Cansi, Y. (2003). PMCC for infrasound data processing. *InfraMatics*, *2*, 1–9.

Le Pichon, A., Ceranna, L., Pilger, C., Mialle, P., Brown, D., Herry, P., & Brachet, N. (2013). The 2013 Russian fireball largest ever detected by CTBTO infrasound sensors. *Geophysical Research Letters*, *40*, 1–6. https://doi.org/10.1002/grl.50619

Le Pichon, A., Ceranna, L., & Vergoz, J. (2012). Incorporating numerical modeling into estimates of the detection capability of the IMS infrasound network. *Journal of Geophysical Research*, *117*(D5), D05121. https://doi.org/10.1029/2011JD016670

Matoza, R. S., Landès, M., Le Pichon, A., Ceranna, L., & Brown, D. (2013). Coherent ambient infrasound recorded by the International Monitoring System. *Geophysical Research Letters*, *40*, 429–433. https://doi.org/10.1029/2012GL054329

McCarty, V. M., & Dalins, I. (1971). Frequency shift in air-coupled surface waves originated by rocket launches. *Journal of Geophysical Research*, *76*(29), 7027–7034. https://doi.org/10.1029/JB076i029p07027

McLaughlin, K. L., Gault, A., & Brown, D. J. (2000). *Infrasound detection of rocket launches* (Technical Report). Science Applications International Corporation (SAIC).

McNutt, S. R., Thompson, G., Brown, R. G., Braunmiller, J., Farrell, A. K., & Mehta, C. (2017). Infrasound and seismic recordings of rocket launches from Kennedy Space Center, 2016-2017. In *American Geophysical Union, Fall Meeting 2017*. American Geophysical Union.

Olson, J. (2012). Infrasound rocket signatures. In *Advanced Maui Optical and Space Surveillance Technologies Conference Proceedings* (pp. 11–14). The Maui Economic Development Board.

Pilger, C., Ceranna, L., & Bönnemann, C. (2017). *Monitoring compliance with the Comprehensive Nuclear-Test-Ban Treaty (CTBT)*. Schweizerbart'sche Verlagsbuchhandlung.

Pilger, C., Ceranna, L., Le Pichon, A., & Brown, P. (2019). Large meteoroids as global infrasound reference events. In *Infrasound Monitoring for Atmospheric Studies* (pp. 451–470). Springer. https://doi.org/10.1007/978-3-319-75140-5\text{_}12

Pilger, C., Gaebler, P., Hupe, P., Ott, T., & Drolshagen, E. (2020). Global monitoring and characterization of infrasound signatures by large fireballs. *Atmosphere*, *11*(1), 83. https://doi.org/10.3390/atmos11010083

Pilger, C., Streicher, F., Ceranna, L., & Koch, K. (2013). Application of propagation modeling to verify and discriminate ground-truth infrasound signals at regional distances. *InfraMatics*, *02*(4), 39–55. https://doi.org/10.4236/inframatics.2013.24004

Silber, E. A., Boslough, M., Hocking, W. K., Gritsevich, M., & Whitaker, R. W. (2018). Physics of meteor generated shock waves in the Earth's atmosphere – a review. *Advances in Space Research*, *62*(3), 489–532. https://doi.org/10.1016/j.asr.2018.05.010

Smith, K. E., Solomon, M. L., Bryan, K. J., Smith, A. O., & Peter, A. M. (2018). Near-field infrasound classification of rocket launch signatures. In *Chemical, Biological, Radiological, Nuclear, and Explosives (CBRNE) Sensing XIX* (Vol. 10629, pp. 106291F). Society of Photo-Optical Instrumentation Engineers. https://doi.org/10.1117/12.2302680

Tahira, M., & Donn, W. L. (1983). Anomalous infrasound from Space Shuttle II and Skylab I. *Journal of the Acoustical Society of America*, *73*(2), 461–464. https://doi.org/10.1121/1.388995

Tenney, S. M., Noble, J. M., Whitaker, R. W., & ReVelle, D. O. (2003). Acoustic/infrasonic rocket engine signatures. In *Unattended Ground Sensor Technologies and Applications V* (Vol. 5090, pp. 30–41). Society of Photo-Optical Instrumentation Engineers. https://doi.org/10.1117/12.487119

Vergoz, J., Le Pichon, A., & Millet, C. (2019). The antares explosion observed by the USArray: An unprecedented collection of infrasound phases recorded from the same event. In *Infrasound monitoring for atmospheric studies* (pp. 349–386). Springer. https://doi.org/10.1007/978-3-319-75140-5\text{_}9